Journal of Colloid and Interface Science 605 (2022) 138–145

Contents lists available at ScienceDirect

Journal of Colloid and Interface Science

journal homepage: www.elsevier.com/locate/jcis

A phase diagram of morphologies for anisotropic particles sculpted from emulsions

Mathew Quinn Giso [a], Haoda Zhao [b], Patrick Thomas Spicer [b], Timothy James Atherton [a,*]

[a] Department of Physics and Astronomy, Tufts University, 574 Boston Ave., Medford, MA 02155, United States
[b] School of Chemical Engineering, University of New South Wales, Union Rd., Kensington, NSW 2033, Australia

GRAPHICAL ABSTRACT

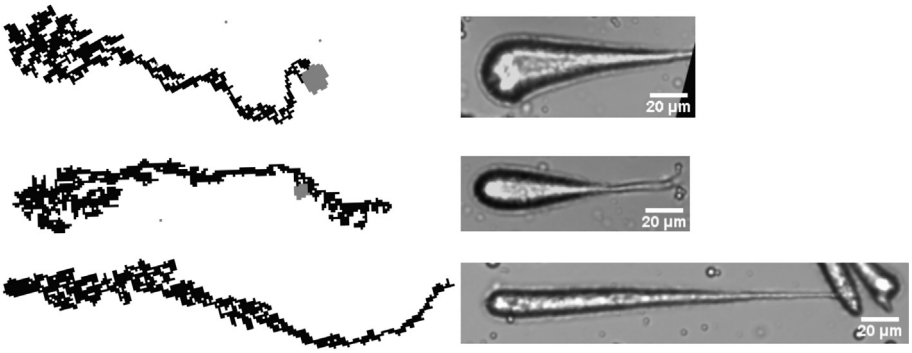

ARTICLE INFO

Article history:
Received 22 January 2021
Revised 7 July 2021
Accepted 8 July 2021
Available online 18 July 2021

Keywords:
Emulsions
Crystallization
Shape control

ABSTRACT

Hypothesis: A micron-scale oil-in-water emulsion droplet frozen in the presence of surfactants can be induced to eject the crystallizing solid from its liquid precursor. This dynamic process produces highly elongated solids whose shape depends critically on the rate of crystallization and the interfacial properties of the tri-phase system.
Experiment: By systematically varying the surfactant concentration and cooling protocol, including quenching from different temperatures as well as directly controlling the cooling rate, we map out the space of possible particle morphologies as a function of experimental control parameters. These results are analyzed using a non-equilibrium Monte Carlo model where crystallization rate and interfacial energies can be specified explicitly.
Findings: Our model successfully predicts the geometry of the resulting particles as well as emergent phenomena including how the particle shape depends on nucleation site and deformation of the precursor droplet during crystallization.

1. Introduction

Oil-in-water emulsions provide an attractive substrate for a variety of synthesis and microfabrication techniques. Emulsion droplets naturally adopt a spherical shape thanks to the strong influence of interfacial tension; enabling the production of capsules or spherical solids with controllable size [1]. Emulsions can

* Corresponding author.
E-mail addresses: mathew.giso@tufts.edu (M.Q. Giso), haoda.zhao@unsw.edu.au (H. Zhao), p.spicer@unsw.edu.au (P.T. Spicer), timothy.atherton@tufts.edu (T.J. Atherton).

https://doi.org/10.1016/j.jcis.2021.07.045
0021-9797/

also be used to synthesize non-spherical shapes by offsetting interfacial tension with elasticity via gelation [2], polymerization [3], or solidification [4]. The creation of many reproducible particle shapes requires some process of shaping, often during assembly [5], through flow in microfluidic channels [1,6], or using molds [7]. Interfacial flows can also shape droplets [8] to produce more complex shapes than continuous flow or molding systems while easing scale-up by using simple emulsion precursors [9–14].

Molten emulsions can be induced to crystallize and, depending on their wettability, crystals may be partially or completely ejected from their precursor droplets. By carefully controlling the interfacial properties of the background, fluid precursor, and crystalline phases through judicious use of surfactants, the growing crystal can be continuously ejected from the precursor. This highly dynamic sculpting process produces elongated crystals referred to as "comets" because, generically, they exhibit an elongated "tail" with a rounded "head" [15]. Tuning the growth conditions by adjusting the surfactant concentration dramatically changes the resulting size and morphology of the particles with aspect ratios from $1-18$ [16].

In this work, we seek to develop a systematic understanding of the possible morphologies that may be achieved with this sculpting process. A qualitative 1D phase diagram, i.e. a map from the parameter space to the resulting comet shapes, proposed in Ref. [15] predicts comet morphology as a function of two rates: the rate of dewetting K_w, i.e. the rate of ejection of crystal from the precursor, and the rate of crystallization K_c. If $K_c \gg K_w$, crystallization proceeds too rapidly for the crystal to be ejected from the precursor and the resulting shape is approximately spherically. Conversely, if $K_w \gg K_c$, crystals form and then are almost immediately ejected leading to small discrete crystals. Comets form in the intermediate regime, $K_c \sim K_w$, when the crystal grows and is ejected at comparable rates.

While this phase diagram is conceptually very helpful, the rates K_c and K_w are not simply related to the actual experimental control parameters, which include the cooling protocol used and the surfactant concentrations as examined in Ref. [16]. Moreover, the process is highly non-equilibrium and stochastic in nature leading to considerable variation even within identically prepared samples. Other factors that could affect comet formation include variation in the contact angle as expected for droplets in motion [17–21] and non-uniform surfactant adsorption which can lead to Marangoni flows [22,23]. A recent review article by Mura and Ding discusses some aspects of this process [24].

To construct a more complete phase diagram, we first develop a phenomenological non-equilibrium Monte Carlo model in Section 2 that includes dewetting and crystallization explicitly and allows us to explore the kinetics of the sculpting process. The model is formulated in terms of parameters that are more closely related to those that can be adjusted experimentally. We map out the phase space in Section 2 and compare our predictions with comets grown as a function of surfactant concentration and crystallization rate in Section 4, including discussion of the growth dynamics and influence of the position of the initial seed on the morphology, and draw conclusions in Section 5.

2. Model

To simulate the sculpting process, illustrated as a series of experimental time resolved snapshots in Fig. 1B, we construct a phenomenological non-equilibrium Monte Carlo model that incorporates dewetting and crystallization behavior, but does not impose any assumptions about the shape of growing crystal or the precursor droplet. Our goal here is to construct a model that predicts the qualitative behavior of the experimental system and hence our treatment of the underlying thermodynamics will be necessarily approximate. Similar models have been widely used to model fluid systems [25–27,17,28,29] because they are easy to implement and can capture a wide range of emergent phenomena.

The dewetting behavior is captured by a conserved 3-state Potts model [30]. The simulation domain is a 2D square lattice with dimensions 251×251. Each lattice site is equipped with a quantity $\sigma_i \in \{b, p, c\}$ indicating the state of the system at that point, where the labels b, p and c refer to background, precursor, and crystal respectively.

The instantaneous energy of the system is given by the Hamiltonian,

$$\mathcal{H} = \gamma \sum_{ij} T_{ij} J_{\sigma_i \sigma_j}, \tag{1}$$

where the topological matrix has entries $T_{ij} = 1$ where sites i and j are connected and zero otherwise. The symmetric matrix $J_{\alpha\beta}$ specifies the interaction energy between sites that have phases α and β,

$$J_{\alpha\beta} = \begin{pmatrix} \gamma_{bb} & \gamma_{bp} & \gamma_{bc} \\ \gamma_{bp} & \gamma_{pp} & \gamma_{pc} \\ \gamma_{bc} & \gamma_{pc} & \gamma_{cc} \end{pmatrix} \tag{2}$$

where the $\gamma_{\alpha\beta}$ are dimensionless and the prefactor γ in (1) has units of energy. The interaction energies are constant during the simulation. This introduces an assumption that the interfacial tensions are constant which experimentally need not be the case. This treatment is consistent with previous work where the changing contact angle was most strongly influenced by gradual depletion of the precursor reservoir [16]. Exploration of time or temperature varying interfacial tensions is left to future work.

During the simulation, the configuration is evolved by exchanging randomly selected neighboring sites (Kawasaki dynamics) preserving the total number of sites in each phase, with the restriction that only exchanges involving precursor and background, i.e. the fluid components of the system, are allowed. Each move changes the energy of the system by ΔE and is accepted with probability P according to the Metropolis Algorithm,

$$P = \begin{cases} 1 & \Delta E \leq 0 \\ \exp(-\Delta\mathcal{H}/kT) & \Delta E > 0 \end{cases}, \tag{3}$$

where kT characterizes the thermal energy of the system.

The model is therefore specified so far by six distinct parameters $\bar{\gamma}_{\alpha\beta} = \gamma_{\alpha\beta}(\gamma/kT)$, but we can exploit the fact that the dynamics (3) only depend on *differences* between these quantities to reduce this number: Since only moves that exchange background and precursor are allowed, ΔE must involve linear combinations of $\bar{\gamma}_{bb} - \bar{\gamma}_{bp}$, $\bar{\gamma}_{bp} - \bar{\gamma}_{pp}$, and $\bar{\gamma}_{pc} - \bar{\gamma}_{bc}$. If we assume for simplicity that the self-interactions are identical, $\bar{\gamma}_{bb} = \bar{\gamma}_{pp}$, and choose them to be zero without loss of generality, then only two parameters, $\bar{\gamma}_{bp}$ and $\Delta\gamma = \bar{\gamma}_{pc} - \bar{\gamma}_{bc}$ remain. The first of these, $\bar{\gamma}_{bp}$, must be positive to promote phase separation of the precursor and background fluids. The second, $\Delta\gamma$, must be positive to achieve dewetting of the crystal from the precursor. Both $\bar{\gamma}_{bp}$ and $\Delta\gamma$ control the rates of their respective process: a higher value of $\bar{\gamma}_{bp}$ implies faster demixing of precursor and background, while a more positive $\Delta\gamma$ increases the rate at which the crystal is ejected from the oil droplet.

Crystallization is incorporated into the model by assuming that growth occurs purely at the crystal-precursor interface without further nucleation events. This is achieved by inclusion of non-equilibrium reaction moves: each time a precursor-crystal pair is randomly selected to flip, the precursor is instead converted to a static crystal site with a probability $P_{p\to c} = e^{\Gamma}$ where $\Gamma < 0$. Decreasing $|\Gamma|$ indicates more rapid crystallization. This mechanic

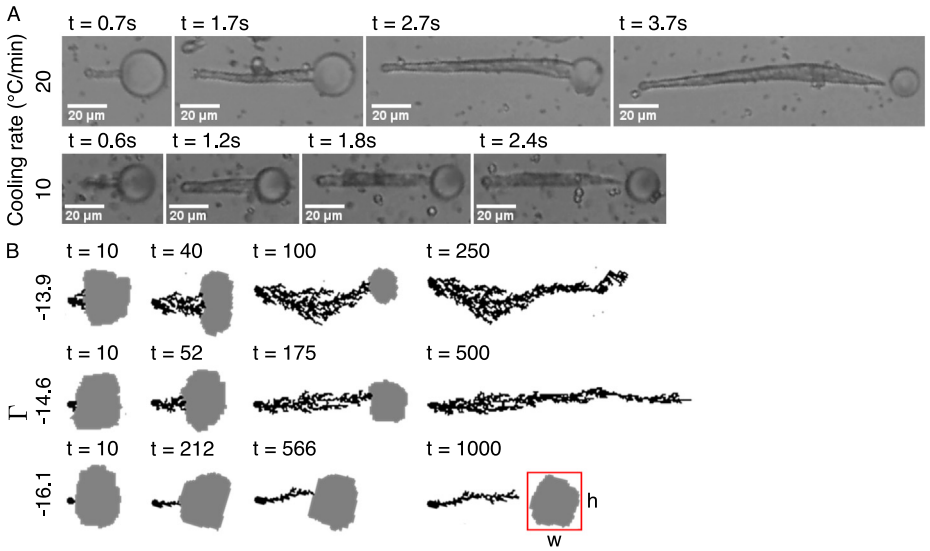

Fig. 1. **A** Time series of crystals from experiment at two different cooling rates with an SDS concentration of 1.5 %wt. **B** Time series of simulation crystals at different Γ, the crystallization rate. Here, the gray sites represent the fluid precursor, and the black sites represent crystal. These time series correspond to the curves in Fig. 6. The time figures are in units of 10^6 Monte Carlo sweeps.

assumes the crystallization does not depend on the number of neighboring crystal sites for the sake of simplicity. Coupling the conversion process to the local environment is an interesting possible target of future work. Given our choice of nearest neighbors, the majority of conversions occur with only one crystal neighbor. This method of implementing crystallization is reminiscent of other work modeling growth processes, such as the Eden Model and other crystallization models [31,32].

Having completed our formulation of the model, we pause to compare and contrast it with the earlier picture proposed in Ref. [15]. Our model generalizes the phase diagram proposed by Ref. [15]. Since $\Delta\gamma$ and Γ are proportional to K_w and K_c, respectively, the single parameter in Ref. [15] that predicts the formation of comets corresponds to a combination of the form $\alpha\Gamma - \beta\Delta\gamma$ where α and β are unknown constants.

3. Methods

Comet preparation— Comets were prepared by creating an emulsion from deionized water, made using a Milli-Q Advantage A10, and two lipids: trihydroxystearin (Peter Cremer, USA) (also known as castor wax), and stearic acid (95%, Sigma–Aldrich). The emulsion was stabilized using a surfactant and cosurfactant: sodium dodecyl sulfate (⩾99.0%, Sigma–Aldrich) and decanol (98%, Sigma–Aldrich).

Comets were prepared in three ways. In all cases, the comet system was prepared by combining a lipid solution and a surfactant solution. Single lipid particles were composed of trihydroxystearin. Mixed lipid particles were composed of trihydroxystearin and stearic acid combined with a 4:6 volume ratio. When combined with the surfactant solution to make an emulsion, the concentration of lipids in the total liquid volume was 0.5 %wt. The solution was heated to 90 °C and stirred well. Surfactant solutions were composed of Milli-Q water, SDS, and decanol. Solutions were prepared at different percent weights of SDS to water. In all cases, decanol was 10% the weight of SDS. Axes labeled %wt sds/decanol follow this convention. (method 1) To observe the crystallization process, the surfactant solution was heated to 90 °C. The lipid and surfactant solutions were then combined and shaken by hand to produce a hot oil-in-water emulsion. In future studies, high-energy stirrers could be used to produce smaller droplets. A drop of the solution was placed on a glass slide and observed with an optical microscope as the system cooled to room temperature. (method 2) To produce crystals in bulk, the surfactant solution was heated to various temperatures depending on the desired quench depth. (method 3) For temperature controlled experiments, the sample's temperature was controlled by a Linkam PE120 Peltier stage. The cooling system was connected to the Linkam stage and an EHEIM professional 4+ water pump. The cooling water was room temperature, 20.5 °C degree. The stage was first set to be 90 °C, and a glass slide with two drops of hot emulsion covered with cover slip was settled on the stage. At this point, the cooling process was initialized and sample collection commenced. In the supplementary material we display the measured temperature as a function of time during three replicate quenching experiments. This shows that the cooling rate for ambient cooling is highly replicable and essentially linear at short times with a slope of roughly 70 °C/min, allowing for direct comparisons between each production method.

A QImaging optiMOS high speed camera was used to record videos for analysis. To create micrographs, a Leica DM2500M microscope and Moticam 10MP digital camera were used. Boxed aspect ratio calculations, and analysis of particle size and shape were performed using imageJ [33–36].

Cluster analysis—The simulated crystals are rarely straight, making metrics like the boxed aspect ratio an incomplete measure of the morphology. To analyze the simulated crystal shape in more detail, we employ the following analysis: working from a site at one end of the crystal, all sites within a specified radius are assigned to a cluster; the center of mass (COM) of this cluster is then calculated and used to identify the next cluster from remaining sites. The process is repeated until all sites in the crystal are assigned to a cluster, yielding a set of clusters and their respective centers of mass. Connecting the COM of adjacent clusters gives a series of line segments which follow the curves of the simulated crystal. The local width of the crystal can be determined as a function of arclength by finding the maximum extent in the normal direction at each point along these line segments. This method produced the length versus width curves shown in the subsequent sections. To average multiple length versus width curves, the mean crystal width was computed as a function of arclength. To find the error bands, we compute the standard deviation in the same way

and add or subtract it from the mean curve. Additionally, an overall aspect ratio can be computed from the maximum width divided by the arclength of the COM graph. We note that this analysis involves one free parameter, the cluster radius r_c, chosen by the operator; we find the resulting profiles $w(s)$ are fairly insensitive to the particular choice if r_c is chosen to be a value of order of the maximum width of the crystal.

To measure the boxed aspect ratio, we identify contiguous sites $\mathbf{x}_i$ belonging to the liquid precursor. We calculate the bounding box from min($\mathbf{x}$) and max($\mathbf{x}$) and display the aspect ratio of the bounding box. This is shown visually in Fig. 1, the red box surrounding the precursor droplet in the lower left indicates how the boxed aspect ratio is calculated. w and h indicate the height and width of the precursor droplet. Dividing these quantities gives the boxed aspect ratio.

4. Results and discussion

4.1. Phase diagram

Using the above model we ran a series of 10 simulations varying Γ and $\Delta\gamma$ and fixing $\bar{\gamma}_{bp} = 2/5$. Simulations are started from an initial state consisting of a circle of 1292 precursor sites surrounded by background host. We will later vary the position of the initial crystal seed sites within the precursor droplet; in this initial section a seed site composed of 21 crystal sites is placed on the background/precursor interface.

Representative results from the ensemble of simulations are shown in Fig. 2A; the aspect ratio of the resulting crystals is calculated as described in the Methods section and is displayed in Fig. 2B. As $\Delta\gamma$ and $|\Gamma|$ are increased, we observe continuous variation of the crystal shape from circular to elongated.

A line that separates circular and elongated crystals is approximately given by $\Gamma = -15 + 4.25\Delta\gamma$, indicated as a dashed red line in Fig. 2A. Intriguingly, for carefully chosen $\Delta\gamma$ and Γ close to this line we find an intermediate regime with moderate aspect ratios $1-4$ not previously observed experimentally. Below a second critical line parallel to the first and indicated in Fig. 2A with a black line, total dewetting occurs such that not all the precursor is used. This results in very small crystals that tend to be very narrow, just 2–3 sites wide, resulting in the very large aspect ratios obtained.

Varying combinations of $\Delta\gamma$ and Γ perpendicular to these two critical lines, i.e. in the direction $\Gamma - \frac{1}{4.25}\Delta\gamma = \text{const.}$, produces the strongest effect on crystal shape. This is consistent with our analysis in the previous section that the combination $\alpha\Gamma - \beta\Delta\gamma$ corresponds to the earlier one-parameter model proposed in Ref. [15]. However, we see there remains significant variation in comet shape in the perpendicular direction: contrast the shape at $(\Delta\gamma, \Gamma) = (0.4, -15)$ with that at $(0.8, -12.7)$ for example.

To test the predictions of this model, we prepare comets as described in the Methods section by systematically varying the quench depth, and hence the crystallization rate, and the concentration of surfactants, and hence the wettability. Representative comet morphologies are shown in Fig. 2C together with a corre-

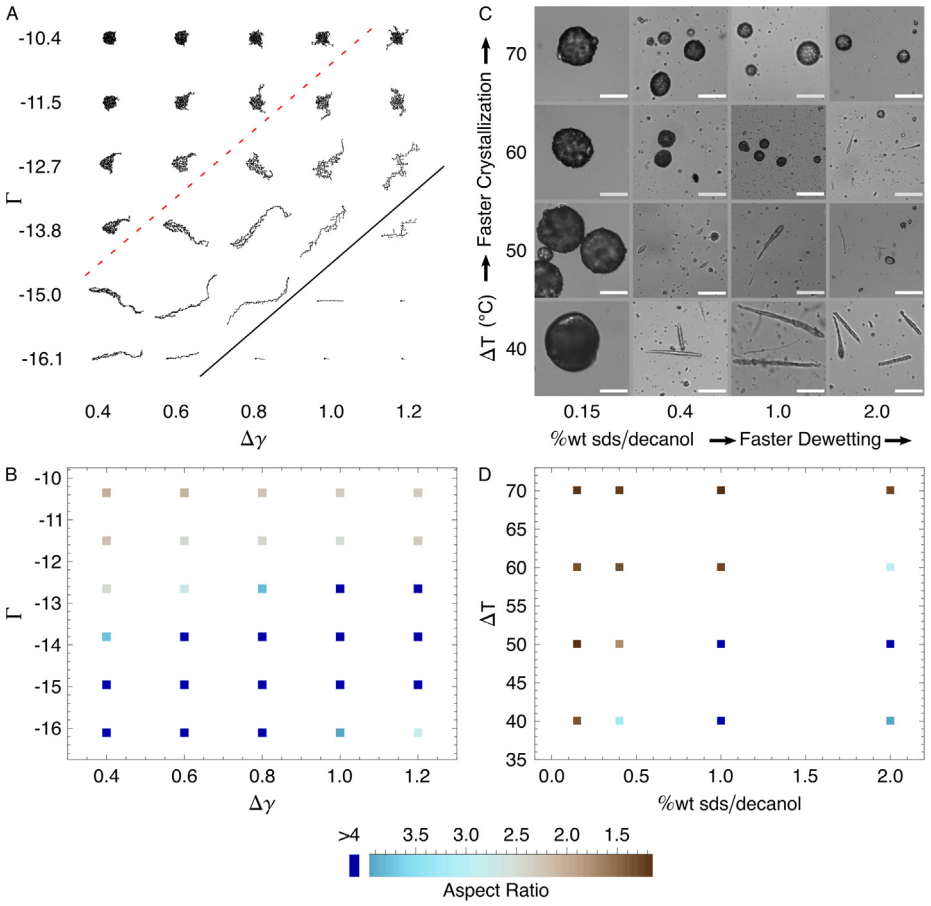

Fig. 2. **A** Simulated crystal shapes as a function of Γ and $\Delta\gamma$ shown on a common scale; some crystals at the lower right did not use the entirety of their precursor reservoir. A line approximately separating circular from elongated morphologies is indicated with dashed red line; the solid black line approximately separates comets from the total dewetting scenario. **B** Aspect ratio of the crystals shown in **A**. **C** Experimental phase diagram showing representative crystals formed at different surfactant concentrations and quench depths. ΔT is the temperature difference between the surfactant and emulsion solution prior to mixing (method 2). The scale bars are 50 μm. **D** Aspect ratio of ensembles of crystals formed.

sponding plot of the aspect ratios in Fig. 2D. The longest crystals formed at low crystallization rates. These crystals were generally between $40-75\mu m$ with the occasional very large and long crystal. Circular morphologies were seen at high crystallization rates and low surfactant concentration. This is consistent with previous work, where ejection was seen at low crystallization rates, but only when the dewetting rate was sufficiently high [15]. In contrast to the theoretical model, where the interfacial energies can be increased as much as the user would like, there is a point where adding additional surfactant will not alter the interfacial tension further. This creates a maximum dewetting rate for a given combination of surfactants.

The experimental trends agree well with the predictions of the Monte Carlo model: circular crystals form independently of surfactant concentration when the crystallization rate is high. As the crystallization rate is reduced, increasing surfactant concentration yields higher aspect ratio crystals, the trend becoming more pronounced as the crystallization rate is reduced further.

To further investigate this behavior, we perform additional experiments using a temperature controlled stage to carefully control the cooling rate. In contrast to the quenching experiments designed to mimic a highly scalable industrial process [37], this method gives better control to probe comet behavior. The results are qualitatively similar, and a phase diagram analogous to Fig. 2C is displayed in Fig. 3. In this diagram, we see robust formation of comets. In our experiments, comets only formed above a minimum concentration approximately equal to the Critical Micelle Concentration for SDS [38] which we use as a natural point of comparison. This is consistent with previous observations [15] and other work on similar systems [39]. Further work should be performed to carefully understand the role of surfactants at low concentrations. New work on droplet motion, for example, indicates possible mechanisms based on micelle-driven depletion effects [22]. The longest crystals observed occurred at a cooling rate of 5 °C/ min and at 1.5%wt surfactant concentration. We also see a distinct change in morphology as the surfactant concentration increases. At 0.8%wt the comets are rod-like, with uniform widths. As the surfactant concentration increases, the comets have much broader heads with long, spindly tails. These additional results collectively indicate that the cooling protocol is important and offers additional possibilities for detailed control of the shape.

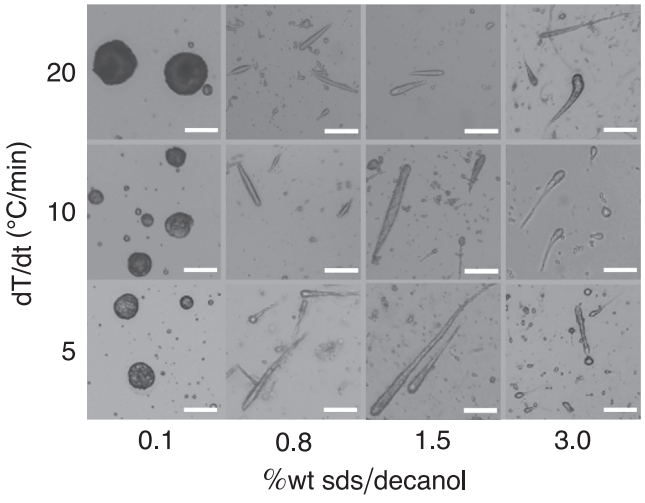

Fig. 3. Crystal formation using a temperature controlled stage (method 3). The vertical axis indicates cooling rate, while the horizontal indicates surfactant concentration as before. Scale bars are 50 μm.

4.2. Droplet profile

We now examine the shape of the comets in more detail. Here, we ran 45 simulations. In the simulations, the width of the crystals depends on the crystallization rate at constant $\Delta\gamma$ even while the length remains roughly constant. In Fig. 4A we show the average contour of crystals formed at different crystallization rates. For rapid crystallization, crystals form a large head with a narrow tail. As the crystallization rate is reduced, the head grows smaller, and the crystals become more uniform, while retaining their high aspect ratio.

We test this prediction by plotting the profile of comets prepared at similar surfactant concentrations but different cooling rates in Fig. 4B. As in the model, the width of the head can be modified by changing the crystallization rate. Notice that the brown curve in Fig. 4B has a different shape than its low $|\Gamma|$ analogue in Fig. 4A. This is likely due to differences between the nucleation sites as will be discussed below. Note that the brown curve in 5B has a more similar geometry.

A second factor governing the shape of the comet is the placement of the initial seed crystal relative to the precursor droplet. Here, we ran 10 simulations. In Fig. 5A we show the profiles of several different comets grown with different initial seed positions. Qualitatively, we can see the crystals formed with central seeds have more prominent heads. This is because the initial placement

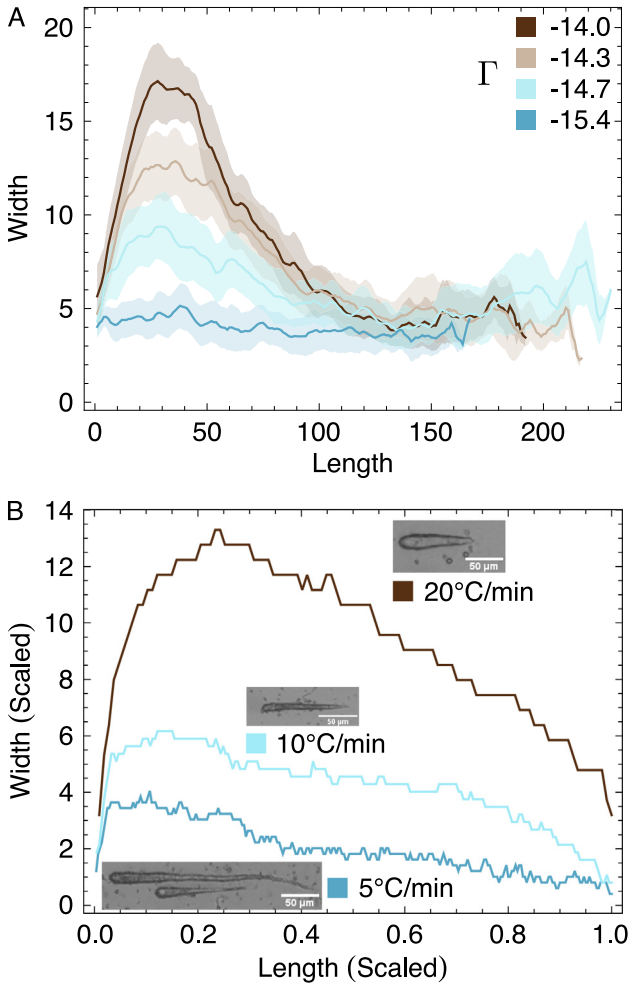

Fig. 4. **A** Width profiles of simulation crystals formed at $\Delta\gamma = 0.73$. Error bands are 1/2 a standard deviation. **B** Width profiles of experimental crystals formed at 1.5 % wt SDS/ decanol (method 3).

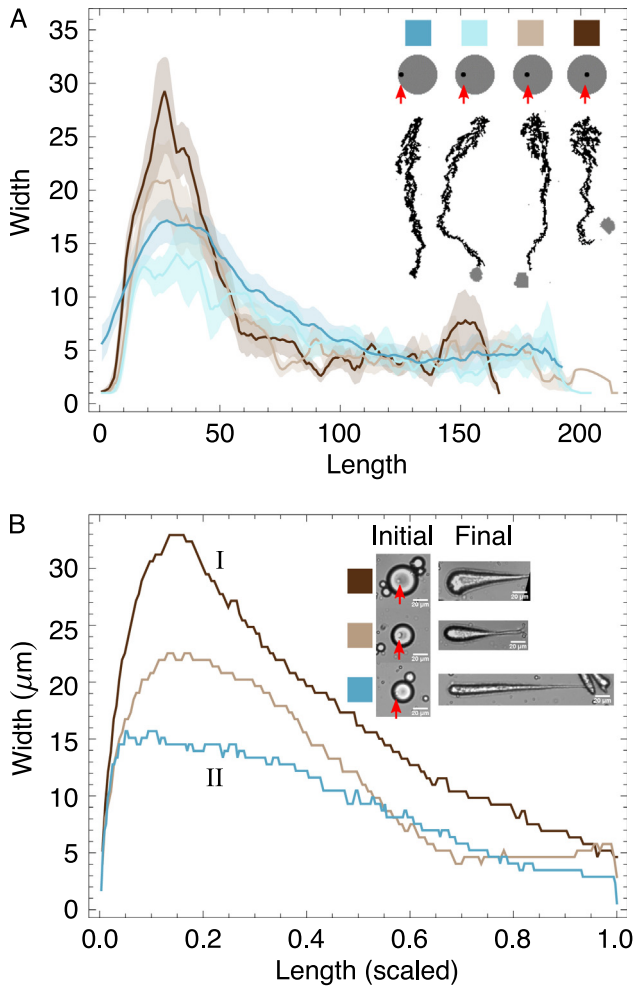

Fig. 5. The shape crystals form as the initial nucleation site changes in **A** simulation and **B** experiment. Simulation crystals were formed at $\Gamma = -14.5$. Error bands are 1/2 a standard deviation. Experimental crystals were formed at 2 %wt SDS solution (method 1). In both figures, red arrows indicate the location of the initial nucleation site.

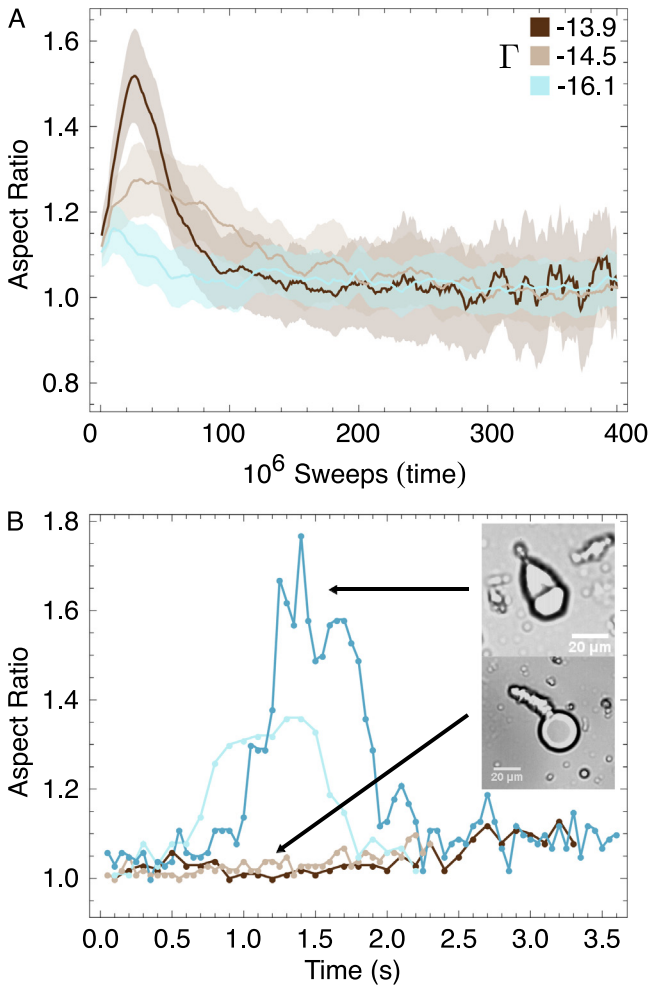

Fig. 6. The boxed aspect ratio of the precursor droplet as a function of time for **A** theory and **B** experiment. In the theory plot, error bands are 1/2 a standard deviation. The experimental crystals were formed with an SDS concentration of 0.6 %wt (method 1).

increases the length of time taken for the droplet to dewet the crystal. During this period, the seed has more time to grow in a uniformly radial manner. This behavior is suppressed as the seed site is moved closer to the edge.

Experimentally, the seed site is a random variable, but we can identify crystals that grew from different seed placements *a posteriori*. We confirm the role of seed site on the head by plotting profiles from a number of observed crystals in Fig. 5B. As our concern here is the crystal shape, we have scaled the widths of the contours to be the same length. Notice that the shape of the neck changes when the nucleation site is close to the center (brown curve labeled I) the crystal has a large head followed by a sharp decrease in width. As the nucleation site moves closer to the edge (blue curve labeled II) the crystals have a more uniform width throughout their length.

4.3. Deformation of precursor droplet

Intriguingly and in contrast to our prior geometric model [16], where the liquid precursor was assumed to remain circular, variation of the precursor droplet shape is observed in simulation. This can be seen visually in the time series shown in Fig. 1. For the $\Gamma = -16.1$ example, the precursor droplet remains spherical. The only real deformation seen is during the initial dewetting. Conversely, at $\Gamma = -13.9$, we see a large deformation of the precursor droplet. We can quantify this by plotting the boxed aspect ratio of the oil droplet (as defined in Methods) as a function of time. The results are shown in Fig. 6A, here each curve is composed of 45 simulation. Error bands are half the standard deviation of the aspect ratio computed at every time interval. We observe a peak in the aspect ratio of the precursor droplet at the initial stages of growth, indicating a large departure from a circular geometry; the magnitude of this peak increases as $|\Gamma|$ decreases. At late times, the precursor droplet is small and can change shape easily leading to the fluctuations on the right side of Fig. 6A. By analyzing the kinetics of the crystal formation obtained by video microscopy, we have also experimentally observed elongation of the precursor droplet as shown in Fig. 6B. Crystals formed with slow ejection (blue curves) exhibit elongated precursor droplets during formation of the head; those formed with fast ejection show precursors that remain circular (brown curves).

5. Conclusion

The central result of this work is a phase diagram describing how tuning the crystallization and dewetting processes can be used to continuously alter the aspect ratio of "comets" formed in crystallizing oil-in-water emulsions. We have established a phase

diagram both theoretically, through a non-equilibrium Monte Carlo model incorporating both processes explicitly, and experimentally by systematically varying quench depth and surfactant concentration. While the model is conceptually simple and in two dimensions, it successfully predicts the structure of the morphology phase diagram including a new intermediate regime of low-aspect ratio droplets, shape variations in the precursor droplet and the importance of nucleation point in determining the shape of the crystal; All of these effects have been observed experimentally. Collectively, our results confirm our hypothesis that crystal morphology can be mapped to a linear combination of cooling rate and surfactant concentration as a proxy for the crystallization rate and the three-phase contact angle.

This work builds upon existing research in a variety of ways. In Ref. [15], the comet shape is conjectured to be the result of competition between relative rates of dewetting and crystallization which are not strongly defined. Our work demonstrates explicitly how the two rates compete. Ref. [16] discusses how variation of the growth angle leads to variation of morphology at different surfactant concentrations. Here, we explore experiments not accessible to a purely geometric model, including how precursor droplet shape and initial nucleation site affect the sculpting process.

The controlled production of shaped colloids has increasing significance to a number of fields of research. Improved control of shaped colloid formation processes is required to enable robust design and prediction of novel particle shapes. While the underlying mechanisms are different, there are numerous publications on shape control with emulsions [40–44]. As discussed in Ref. [42], the resulting shape is dependent on the choice of oil and surfactant. Our system is unique in that due to our use of two surfactants we get much stronger ejection behavior [39,45]. This results in a solidification front similar to the freezing of sessile droplets [46] which is not common in other emulsion shape control research. Further, the simulation results enable understanding of how detailed aspects of particle shape, like tapering and curvature, form during emulsion crystallization. As applications of shaped particles increase and require specific features or dimensions, our model will provide guidelines for experimental design and optimization to improve shape control and production.

CRediT authorship contribution statement

Mathew Quinn Giso: Methodology, Software, Formal analysis, Investigation, Data curation, Writing - original draft, Visualization. **Haoda Zhao:** Methodology, Formal analysis, Investigation, Writing - review & editing. **Patrick Thomas Spicer:** Conceptualization, Resources, Writing - review & editing, Project administration, Funding acquisition. **Timothy James Atherton:** Conceptualization, Writing - original draft, Writing - review & editing, Supervision, Project administration, Funding acquisition.

Declaration of Competing Interest

The authors declare that they have no known competing financial interests or personal relationships that could have appeared to influence the work reported in this paper.

Acknowledgments

This material is based upon work supported by the National Science Foundation under grant DMR-1654283 and the Tufts International Research Program. The authors also acknowledge partial support from the Australian Government through the Australian Research Council's Discovery Projects funding scheme, Project DP150100865.

Appendix A. Supplementary material

Supplementary data associated with this article can be found, in the online version, at https://doi.org/10.1016/j.jcis.2021.07.045.

References

[1] R.K. Shah, H.C. Shum, A.C. Rowat, D. Lee, J.J. Agresti, A.S. Utada, L. Chu, J. Kim, A. Fernandez-Nieves, C.J. Martinez, D.A. Weitz, Designer emulsions using microfluidics, Mater. Today 11 (2008) 18–27.
[2] A. Pawar, M. Caggioni, R. Hartel, P. Spicer, Arrested coalescence of viscoelastic droplets with internal microstructure, Faraday Discuss. 158 (2012) 341–350.
[3] D. Dendukuri, S.S. Gu, D.C. Pregibon, T.A. Hatton, P.S. Doyle, Stop-flow lithography in a microfluidic device, Lab Chip 7 (7) (2007) 818–828.
[4] H. Bunjes, M.H.J. Koch, K. Westesen, Effect of Particle Size on Colloidal Solid Triglycerides, Langmuir 16 (2000) 5234.
[5] T. Schneider, S. Mandre, Algorithm for a Microfluidic Assembly Line, Phys. Rev. Lett. 106 (9) (2011) 94503.
[6] T.A. Prileszky, E.M. Furst, Crystallization Kinetics of Partially Crystalline Emulsion Droplets in a Microfluidic Device, Langmuir 32 (2016) 5141–5146, https://doi.org/10.1021/acs.langmuir.6b00420.
[7] J.K. Nunes, S.E.A. Gratton, K.P. Herlihy, P.D. Pohlhaus, J.M. DeSimone, Fabrication of multiphasic and regio-specifically functionalized PRINT particles of controlled size and shape, New J. Phys. 11 (2009) 75018.
[8] R.C. Hayward, A.S. Utada, N. Dan, D.A. Weitz, Dewetting Instability during the Formation of Polymersomes from Block-Copolymer-Stabilized Double Emulsions, Langmuir 22 (10) (2006) 4457–4461.
[9] I. Kralova, J. Sjöblom, Surfactants used in food industry: a review, J. Dispersion Sci. Technol. 30 (9) (2009) 1363–1383.
[10] R.S. Lam, M.T. Nickerson, Food proteins: a review on their emulsifying properties using a structure–function approach, Food Chem. 141 (2) (2013) 975–984.
[11] O.D. Velev, A.M. Lenhoff, E.W. Kaler, A class of microstructured particles through colloidal crystallization, Science 287 (5461) (2000) 2240–2243.
[12] U. Kedar, P. Phutane, S. Shidhaye, V. Kadam, Advances in polymeric micelles for drug delivery and tumor targeting, Nanomedicine: Nanotechnology, Biol. Med. 6 (6) (2010) 714–729.
[13] W. Kaialy, A. Alhalaweh, S.P. Velaga, A. Nokhodchi, Effect of carrier particle shape on dry powder inhaler performance, Int. J. Pharmaceut. 421 (1) (2011) 12–23.
[14] K. Gilbertson, W. Finlay, C. Lange, M. Brett, D. Vick, Nanofabrication of high aspect ratio aerosol particles for deposition studies in a model human airway, in: 2004 International Conference on MEMS, NANO and Smart Systems (ICMENS'04), IEEE, pp. 268–270.
[15] P.T. Spicer, R.W. Hartel, Crystal comets: Dewetting during emulsion droplet crystallization, Austral. J. Chem. 58 (9) (2005) 655–659.
[16] M.Q. Giso, H. Zhao, P.T. Spicer, T.J. Atherton, Crystal comets: A geometric model for sculpting anisotropic particles from emulsions, Langmuir 36 (46) (2020) 13853–13859.
[17] V. Mortazavi, R.M. D'Souza, M. Nosonovsky, Study of contact angle hysteresis using the cellular potts model, PCCP 15 (8) (2013) 2749–2756.
[18] P.-G. De Gennes, Wetting: statics and dynamics, Rev. Modern Phys. 57 (3) (1985) 827.
[19] A. Marmur, C. Della Volpe, S. Siboni, A. Amirfazli, J.W. Drelich, Contact angles and wettability: Towards common and accurate terminology, Surface Innovat. 5 (1) (2017) 3–8.
[20] L. Gao, T.J. McCarthy, Contact angle hysteresis explained, Langmuir 22 (14) (2006) 6234–6237.
[21] D. Bonn, J. Eggers, J. Indekeu, J. Meunier, E. Rolley, Wetting and spreading, Rev. Modern Phys. 81 (2) (2009) 739.
[22] C. Jin, C. Krüger, C.C. Maass, Chemotaxis and autochemotaxis of self-propelling droplet swimmers, Proc. Nat. Acad. Sci. 114 (20) (2017) 5089–5094.
[23] D. Quéré, Fluid coating on a fiber, Annu. Rev. Fluid Mech. 31 (1) (1999) 347–384.
[24] E. Mura, Y. Ding, Nucleation of melt: From fundamentals to dispersed systems, Adv. Colloid Interface Sci. 102361 (2021).
[25] V. Tikare, J.D. Cawley, Application of the potts model to simulation of ostwald ripening, J. Am. Ceram. Soc. 81 (3) (1998) 485–491.
[26] S. Ljunggren, J.C. Eriksson, Shape fluctuations of spherical micelles, J. Chem. Soc., Faraday Trans. 2: Mol. Chem. Phys. 80 (4) (1984) 489–497.
[27] R.P. Sear, Nucleation at contact lines where fluid-fluid interfaces meet solid surfaces, J. Phys.: Condens. Matter 19 (46) (2007) 466106.
[28] Z. Xu, J. Lioi, J. Mu, M.M. Kamocka, X. Liu, D.Z. Chen, E.D. Rosen, M. Alber, A multiscale model of venous thrombus formation with surface-mediated control of blood coagulation cascade, Biophys. J.s 98 (9) (2010) 1723–1732.
[29] D.W. Cheong, A.Z. Panagiotopoulos, Monte carlo simulations of micellization in model ionic surfactants: Application to sodium dodecyl sulfate, Langmuir 22 (9) (2006) 4076–4083.
[30] M.E.J. Newman, G.T. Barkema, Monte Carlo methods in statistical physics, Clarendon Press; Oxford University Press, Oxford New York, 1999.
[31] M.L. Mansfield, L.I. Klushin, A generalized eden model of polymer crystallization, Polymer 35 (14) (1994) 2937–2943.
[32] K.A. Jackson, G.H. Gilmer, D.E. Temkin, J.D. Weinberg, K. Beatty, Non-equilibrium phase transformations, J. Crystal Growth 128 (1–4) (1993) 127–138.

[33] D.L. Williams, A.T. Kuhn, M.A. Amann, M.B. Hausinger, M.M. Konarik, E.I. Nesselrode, Computerised measurement of contact angles, Galvanotechnik 101 (11) (2010) 2502.
[34] G. Lamour, A. Hamraoui, A. Buvailo, Y. Xing, S. Keuleyan, V. Prakash, A. Eftekhari-Bafrooei, E. Borguet, Contact angle measurements using a simplified experimental setup, J. Chem. Educat. 87 (12) (2010) 1403–1407.
[35] C.A. Schneider, W.S. Rasband, K.W. Eliceiri, Nih image to imagej: 25 years of image analysis, Nature Methods 9 (7) (2012) 671.
[36] J. Schindelin, I. Arganda-Carreras, E. Frise, V. Kaynig, M. Longair, T. Pietzsch, S. Preibisch, C. Rueden, S. Saalfeld, B. Schmid, Fiji: an open-source platform for biological-image analysis, Nature Methods 9 (7) (2012) 676.
[37] R.K. Panandiker, K.A. Vetter, D.S. Dunlop, K.G. Braeckman, K.J.M. Depoot, T.R.M. Vanpachtenbeke, Liquid treatment composition comprising a pearlescent agent, uS Patent 7,910,535 (March 2011).
[38] E. Fuguet, C. Ràfols, M. Rosés, E. Bosch, Critical micelle concentration of surfactants in aqueous buffered and unbuffered systems, Anal. Chim. Acta 548 (1–2) (2005) 95–100.
[39] K. Boode, P. Walstra, Partial coalescence in oil-in-water emulsions 1. nature of the aggregation, Colloids Surf., A 81 (1993) 121–137.
[40] D. Yang, A.N. Hrymak, Crystal morphology of hydrogenated castor oil in the crystallization of oil-in-water emulsions: Part i. effect of temperature, Ind. Eng. Chem. Res. 50 (20) (2011) 11585–11593.
[41] D. Yang, A.N. Hrymak, M.R. Kamal, Crystal morphology of hydrogenated castor oil in the crystallization of oil-in-water emulsions: Part ii. effect of shear, Ind. Eng. Chemi. Res. 50 (20) (2011) 11594–11600.
[42] N. Denkov, S. Tcholakova, I. Lesov, D. Cholakova, S.K. Smoukov, Self-shaping of oil droplets via the formation of intermediate rotator phases upon cooling, Nature 528 (7582) (2015) 392–395.
[43] D. Cholakova, N. Denkov, S. Tcholakova, I. Lesov, S.K. Smoukov, Control of drop shape transformations in cooled emulsions, Adv. Colloid Interface Sci. 235 (2016) 90–107.
[44] D. Cholakova, Z. Valkova, S. Tcholakova, N. Denkov, S.K. Smoukov, self-shaping of multicomponent drops, Langmuir 33 (23) (2017) 5696–5706.
[45] K. Boode, P. Walstra, A. de Groot-Mostert, Partial coalescence in oil-in-water emulsions 2. Influence of the properties of the fat, Colloids Surf., A 81 (1993) 139–151.
[46] D. Anderson, M.G. Worster, S.H. Davis, The case for a dynamic contact angle in containerless solidification, J. Crystal Growth 163 (3) (1996) 329–338.